Sustainability in Environment
ISSN 2470-637X (Print) ISSN 2470-6388 (Online)
Vol. 11, No. 3, 2026
www.scholink.org/ojs/index.php/se

Original Paper

Research on the Antibacterial Properties of Stone Heritage Buildings

Shengyu Yang[1]

[1] Guizhou Minzu University, Guiyang City, Guizhou Province, China

Received: April 27, 2026 Accepted: May 29, 2026 Online Published: June 1, 2026

doi:10.22158/se.v12n3p75 URL: http://dx.doi.org/10.22158/se.v12n3p75

Abstract

The disinfection of stone heritage buildings poses a major challenge in global heritage conservation. Currently, the lack of effective antibacterial agents to inhibit the growth of microorganisms on stone buildings necessitates urgent exploration of effective and green methods to eliminate fungi and bacteria colonizing the surfaces of stone heritage structures. Therefore, this study synthesized silver nanoparticles using aqueous and alcoholic extracts from four plant species and evaluated their antibacterial properties. Experimental results showed that eight types of biosynthesized silver nanoparticles, particularly those synthesized using cinnamon extract, exhibited excellent antibacterial effects against Escherichia coli, Staphylococcus aureus, Aspergillus niger, and Aspergillus flavus. These plant-mediated silver nanoparticles were synthesized under different reaction conditions and characterized by UV spectroscopy and other techniques. The results demonstrated that silver nanoparticles synthesized with cinnamon extract, in particular, showed superior antibactrial performance against E. coli, S. aureus, A. niger, and A. flavus compared to conventional chemically synthesized silver nanoparticles and the chemical biocide benzalkonium chloride (BC). This study confirms that plant-mediated synthesis of silver nanoparticles is a feasible and green antibacterial agent for application on stone heritage buildings.

Keywords

Stone buildings, Plant-mediated silver nanoparticles, Antibacterial effect, Benzalkonium chloride

1. Introduction

Microbial deterioration of stone heritage buildings is a widespread phenomenon globally, particularly in open-air environments (DENG S, TING, 2005; FAN Y, LI Y, LI H, et al., 2018; FU, JIANG, CHAO et al., 2022). These microorganisms mainly include bacteria, fungi, lichens, and algae, with bacteria being the most abundant group. Among the common microbial communities found on stone heritage

buildings are *Escherichia coli*, *Staphylococcus aureus*, *Aspergillus niger*, and *Aspergillus flavus*. *E. coli* secretes metabolites such as organic acids that react with minerals in the stone, leading to changes in the chemical composition and structure of the stone heritage, thereby affecting its state of preservation. The destructive effect of *S. aureus* on stone heritage is mainly reflected in its ability to form biofilms, which alter the microenvironment on the stone surface, causing changes in the physical and chemical properties of the stone. *Aspergillus niger* can form colonies on the stone surface, resulting in black discoloration of the stone heritage surface and darkening of the gypsum crust on calcium-containing stones. The growth of *Aspergillus flavus* on the stone surface leads to color changes and erosion. Therefore, research on antimicrobial strategies against microorganisms on stone heritage is of great significance for heritage conservation (AN, WU, SHI et al., 2021; ANAE, AHMAD, KUMAR et al., 2021; BOUSKOUT, BOURHIA, AL FEDDY et al., 2022).

We found that among ten plant extracts, those from cinnamon leaf, clove leaf, thyme leaf, and agastache leaf exhibited particularly significant bactericidal effects. These highly effective plant extracts can also act synergistically with silver nanoparticles to effectively eliminate biodeteriogens within stone heritage buildings. Hence, this study selected these four plants with strong bactericidal properties as bioreducing agents for the synthesis of silver nanoparticle-based fungicides. The prepared silver nanomaterials, combined with plant extracts, were applied in biodeterioration simulation experiments under laboratory conditions. The four common microbial strains mentioned above were purchased from the market as the targets for antimicrobial performance testing in this study. Their efficacy was compared with that of the traditional chemical biocide benzalkonium chloride, in order to investigate the antimicrobial properties of plant-synthesized silver nanoparticle extracts applied to stone heritage buildings (HAN, AN, LIU et al., 2023; HOU, ZHU, WANG et al., 2024; HUANG, LI, WU et al., 2015).

2. Method

2.1 Study Area

This study selected the Yunfeng Tunpu, located 18 km south of Anshun City, Guizhou Province, China, as the research area. This region is characterized by its karst landforms, mountainous plateau hills, and low-to-medium mountain terrain. It is also renowned for its unique traditional stone-built architectural style and pleasant climatic conditions. In 2001, Yunfeng Tunpu was designated as a National Key Cultural Relics Protection Unit. Yunfeng Tunpu is a settlement of the descendants of military personnel and civilians from the Ming Dynasty war period. After six hundred years of historical heritage and evolution, it has gradually developed into an ancient architectural complex primarily constructed from limestone[10-13]. However, due to the significant impact of biological weathering in this area, some buildings have already exhibited notable aesthetic changes and stone damage, being severely deteriorated by microorganisms (Figure 1).

Figure 1. The Current Status of Biological Degradation in Yunfeng Tunpu is Marked as Aesthetic Damage and Stone Damage

2.2 Preparation of Plant Extracts

First, the cleaned and dried plant leaves (cinnamon leaves, clove leaves, thyme leaves, and agastache leaves, all purchased from a local supermarket) were pulverized. For each type of leaf, 10 g of powder was weighed and added to 100 mL of deionized water and 100 mL of 99.7% anhydrous ethanol solution, respectively. Subsequently, these mixtures were heated in a water bath at 80°C for 30 minutes. After heating, the solutions were centrifuged at a speed of 10,000 r/min, and the supernatants were collected. Finally, the extracts were filtered through Whatman Grade 1 filter paper to obtain the aqueous extract and the alcoholic extract for each type of leaf (LENG, YUAN, ZENG et al., 2015; LI, B., LI, K., & LI, X., 2024; LI, H., QU, Y., WANG, Z. et al., 2022).

2.3 Optimization Procedure of Silver Nanoparticles

To improve the yield and antibacterial effect of silver nanoparticles, we optimized the reaction conditions between plant extracts and $AgNO_3$ through single-factor controlled experiments.

Temperature effect experiment: The volume ratio of plant extract to $AgNO_3$ was kept constant, while the reaction temperature was varied, and the reaction was observed over a fixed period. After the reaction, the solution was measured using a UV-visible spectrophotometer, and the spectral data in the wavelength range of 250-600 nm were recorded.

Volume ratio effect experiment: The reaction temperature was kept constant, while the volume ratio of plant extract to $AgNO_3$ was varied, and the reaction was observed over a fixed period. The solution was similarly measured using a UV-visible spectrophotometer, and the spectral data were recorded.

After the experiments, the reaction solution was centrifuged to separate the precipitate, which was then subjected to a second centrifugation until the supernatant became clear. The precipitate was dried, and the silver nanoparticles were weighed. Solutions of different concentrations were prepared for subsequent experiments. Meanwhile, benzalkonium chloride (BC) was used as a control group. The entire preparation process is shown in Figure 2.

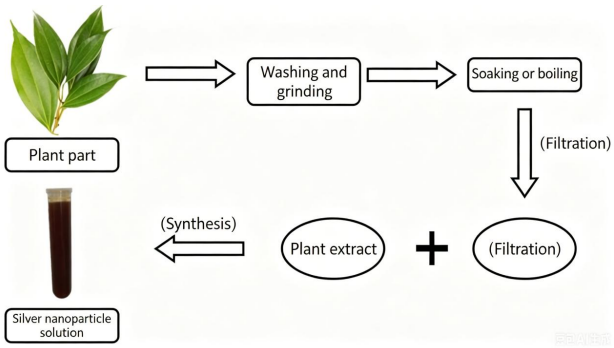

Figure 2. Flowchart of Nanosilver Synthesized from Plants

2.4 Green Synthesis of Silver Nanoparticles

After cleaning the plant leaves and air-drying them at room temperature, the four types of plant leaves were separately crushed using a grinder. For each type of leaf, 10 g of powder was weighed and added to 100 mL of deionized water and 100 mL of ethanol solution, respectively. After heating at 80°C for 30 minutes, the solution was centrifuged at 10,000 rpm. The supernatant was collected and filtered through Whatman Grade 1 filter paper to obtain the aqueous and alcoholic extracts of the plant leaves.

Then, 9 mL of plant extract was added to 10 mL of silver nitrate solution and heated continuously at 90°C for 150 minutes. Changes in the solution color were observed. Subsequently, the resulting solution was measured using a UV-visible spectrophotometer in the wavelength range of 250–600 nm. After centrifugation at 10,000 rpm for 20 minutes, the supernatant was removed and the precipitate was retained. Then, 5 mL of deionized water was added for a second centrifugation, repeated until the solution became colorless. The precipitate was placed in an oven at 60°C and dried for 24 hours, then removed. The characteristics of the silver nanoparticles were observed using a scanning electron microscope and other instruments. Finally, the silver nanoparticles were weighed and reagents of corresponding concentrations (1 μg/mL, 3 μg/mL, 5 μg/mL) were prepared and stored for later use.

(We defined: CWAg as silver nanoparticles synthesized from cinnamon aqueous extract; CAAg as silver nanoparticles synthesized from cinnamon alcoholic extract; SWAg as silver nanoparticles synthesized from clove aqueous extract; SAAg as silver nanoparticles synthesized from clove alcoholic

extract; TWAg as silver nanoparticles synthesized from thyme aqueous extract; TAAg as silver nanoparticles synthesized from thyme alcoholic extract; PWAg as silver nanoparticles synthesized from agastache aqueous extract; PAAg as silver nanoparticles synthesized from agastache alcoholic extract; BC as benzalkonium chloride. (MA, ZHU, NIE et al., 2021; MAI, TANG, TANG et al., 2025)

2.5 Antibacterial Performance Testing of Silver Nanoparticles

To evaluate the antibacterial effects of silver nanoparticles against Escherichia coli, Staphylococcus aureus, Aspergillus niger, and Aspergillus flavus, these microbial strains were purchased from a local market. First, the strains were subjected to gradient dilution to achieve a concentration of 10^6 cells per milliliter. LB agar medium and potato dextrose agar (PDA) medium were prepared, sterilized by autoclaving at 120°C for 20 minutes, and then cooled to 36°C. Subsequently, sterile swabs were used to inoculate E. coli and S. aureus onto LB solid medium, and A. niger and A. flavus onto PDA solid medium. Six wells were set in each microbial culture medium. The five peripheral wells were each injected with 150 μL of different biocides, including silver nanoparticle solution (3 μg/mL) and benzalkonium chloride (0.3%), while the central well served as a control group with no additive. The treated cultures were incubated at 36°C for two days. After the formation of inhibition zones, the diameters of the inhibition zones were measured using a vernier caliper to evaluate the antibacterial activity of the silver nanoparticles (MARCIŃCZYK, KRASUCKA, DUAN et al., 2024).

2.6 Data Processing

All experimental data described above were recorded using Excel 2016. All mean values were calculated from at least three independent experiments and are expressed as mean ± standard deviation. The generation information of silver nanoparticles was visualized using Origin 2022. Statistical significance was analyzed using non-parametric tests in IBM SPSS 27.0.1. Each experimental value was compared with its corresponding control value at each test point. A p-value < 0.05 was considered statistically significant.

3. Results

3.1 Characterization of Silver Nanoparticles

When the $AgNO_3$ solution came into contact with the plant extracts, a color change occurred in the solution. As the water bath temperature and reaction time increased, the color gradually deepened. The color changes were as follows: the aqueous extract of cinnamon and the alcoholic extract of agastache reacted with $AgNO_3$, with the color changing from light green to dark brown and light yellow, respectively; the alcoholic extract of cinnamon, the alcoholic extract of clove, and the alcoholic extract of thyme reacted with $AgNO_3$, with the color changing from dark green to brown, light brown, and dark brown, respectively; after adding the $AgNO_3$ solution to the aqueous extract of clove, the color changed from brown to light brown; after adding the $AgNO_3$ solution to the aqueous extract of thyme, the color changed from orange to dark brown; after adding the $AgNO_3$ solution to the aqueous extract of agastache, the color changed from yellow to light brown.

Brown coloration is a distinctive feature of the surface plasmon resonance (SPR) of silver nanoparticles. The appearance of this color indicates the formation of silver nanoparticles. In other studies, using aqueous extracts of clove leaves and thyme leaves as reducing agents, a brown color was also produced after reaction with $AgNO_3$, and the synthesis of silver nanoparticles was confirmed by instrumental analysis. This suggests that the mixture of $AgNO_3$ and plant extracts in this experiment may also have synthesized silver nanoparticles.

In this experiment, after the $AgNO_3$ solution came into contact with different plant extracts, the solution color gradually deepened with increasing water bath temperature and reaction time, indicating the formation of silver nanoparticles. UV-visible spectroscopic analysis showed that the eight types of silver nanoparticles formed their own unique absorption curves, with different maximum absorbance values in the wavelength range of 420–450 nm. Among them, TAAg and CAAg exhibited the highest absorbance peaks, CWAg showed the narrowest curve, and TWAg showed the broadest curve, indicating differences in silver nanoparticle content, particle size uniformity, and polydispersity. The strong absorption band detected by UV-visible spectroscopy is attributed to the surface plasmon resonance (SPR) phenomenon of silver nanoparticles, whose position and shape are influenced by the medium, particle characteristics, and surface-adsorbed substances. Although particle size was not directly measured, based on the positions of the absorption peaks, it can be estimated that the particle sizes of silver nanoparticles of CWAg, CAAg, PAAg, TAAg, and PWAg in this experiment may range between 35–80 nm.

3.2 Optimization Results of Plant-Synthesized Silver Nanoparticles Reaction Time

With increasing reaction time, the absorbance of CWAg increased, indicating a rise in the yield of silver nanoparticles, with peaks reached at 150 min and 180 min (Figure 3). For CAAg, at a volume ratio of 9:1 and 90°C, the maximum absorbance was achieved after 120 min, after which the peak value decreased accompanied by a red shift phenomenon (Figure 4i), which may be attributed to the aggregation of silver nanoparticles. For SWAg, TWAg, and PWAg, absorption curves began to form after 15 min, with symmetrical distribution at 30 min. As time increased, the absorbance values rose and the distribution broadened (Figures 5d, 7d, 9d). For SAAg, no obvious absorption curve was observed before 30 min, but the absorbance increased with time, reaching a maximum at 180 min (Figure 5d). For PAAg, under conditions of 90°C and volume ratios of 9:1 or 8:2, the optimal reaction times were 150 min and 180 min (Figures 10k, 10i).

Reaction Volume Ratio

In the experiments where different volume ratios of $AgNO_3$ to plant extracts were used for silver nanoparticle synthesis, it was found that CWAg produced absorption peaks under all tested conditions (Figure 3). Among these, the highest absorption peak was observed at a ratio of 8:2, indicating the generation of more silver nanoparticles, while the lowest absorption peak was observed at a ratio of 6:4. For SWAg and TWAg, no obvious absorption peaks were observed at the 6:4 ratio (Figures 5 and 7), possibly because the high content of reducing substances in the plant extracts continued to participate

in the reaction after reducing the silver ions, interfering with the synthesis of silver nanoparticles. At the 7:3 ratio, most solutions produced absorption peaks only under specific conditions, indicating that this ratio is unsuitable for the synthesis of most silver nanoparticles. The experimental data showed that the 9:1 and 8:2 ratios generated uniformly distributed absorption curves, which is consistent with the observation that higher volume ratios of silver precursor solution to plant extract favor the generation of silver nanoparticles. The difficulty in forming uniform absorption curves at the 6:4 and 7:3 ratios may be attributed to insufficient contact between silver ions and the reducing substances in the plant extracts, as well as the possible presence of excess oxidizing substances in the plant extracts that re-oxidize the reduced silver atoms, thereby affecting the stable formation of silver nanoparticles.

Reaction Temperature

The experimental results indicate that the synthesis efficiency of silver nanoparticles is significantly related to the reaction temperature. Under a volume ratio of $AgNO_3$ to plant extract of 9:1, as the temperature increased from 70°C to 90°C, the maximum absorbance peak of CWAg increased from 0.27 to 0.78 (Figure 3d, h, i), indicating that the yield of silver nanoparticles increased with rising temperature. A similar trend was observed in other volume ratios. For example, for PWAg at a ratio of 6:4, distinct absorption peaks were observed at 80°C and 90°C, but not at 70°C. However, for certain plant extracts such as TW, at a ratio of 8:2, a strong absorption peak formed at 80°C, but further temperature increase led to a decrease in the absorption peak value (Figure 7c, g), indicating a reduction in yield. This suggests that different plant extracts have their own optimal temperature thresholds; exceeding these thresholds may lead to non-uniform particle sizes and poor antibacterial performance. Therefore, based on the comprehensive experimental data, the optimal reaction times were determined to be 30 min, 120 min, 150 min, and 180 min; the optimal volume ratios were 9:1 and 8:2; and the optimal reaction temperatures were 80°C and 90°C. These conditions contribute to improving the synthesis efficiency and yield of silver nanoparticles.

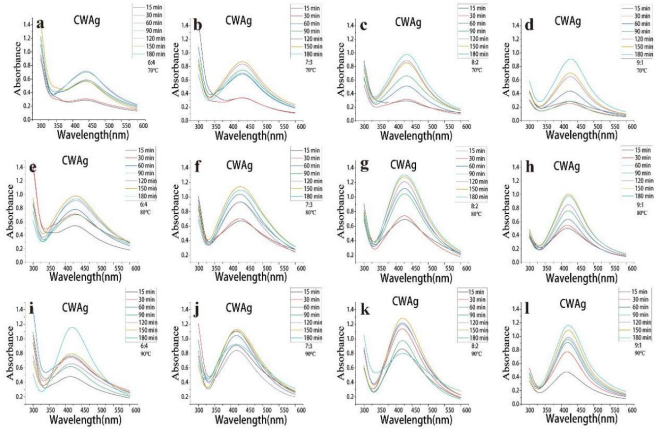

Figure 3. UV Spectra of Nanosilver Synthesized from Aqueous Extract of Cinnamon under One Factor Control

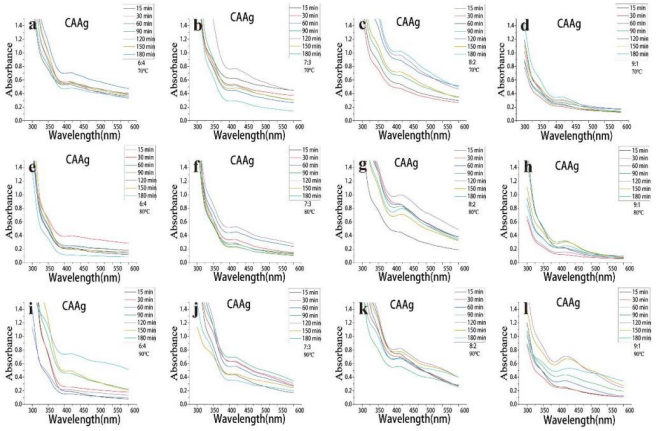

Figure 4. UV Spectra of Nanosilver Synthesized from Alcoholic Extract of Cinnamon under One Factor Control

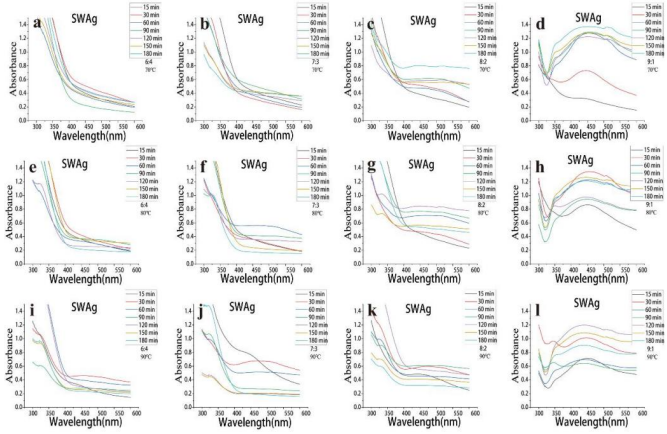

Figure 5. UV Spectra of Nanosilver Synthesized from Aqueous Extract of Clove under One-factor Control

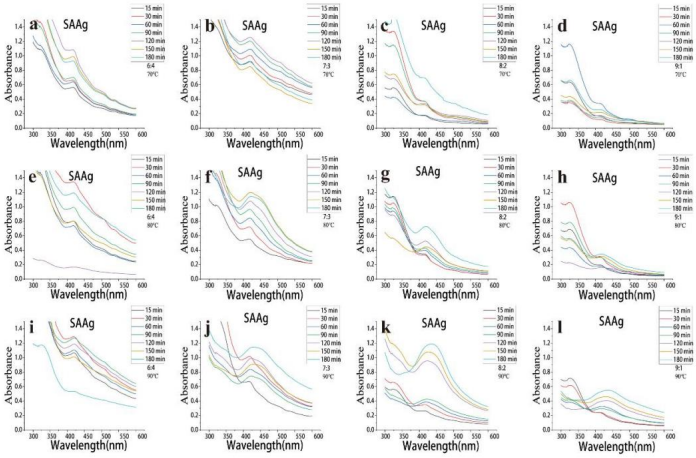

Figure 6. UV Spectra of Nanosilver Synthesized from Alcoholic Extract of Clove under One Factor Control

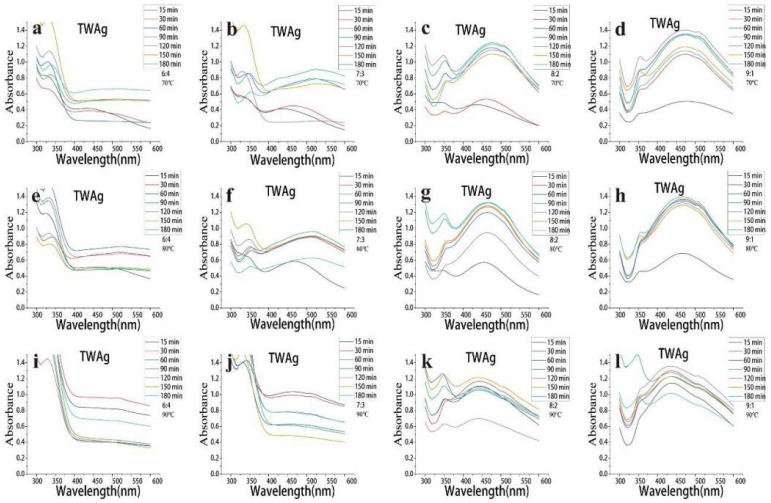

Figure 7. UV Spectra of Nanosilver Synthesized from Aqueous Extract of Thyme under One Factor Control

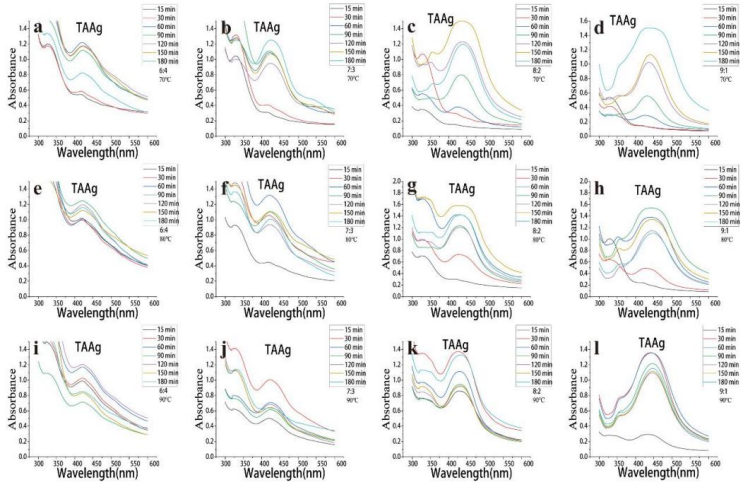

Figure 8. UV Spectra of Nanosilver Synthesized from the Alcoholic Extract of Thyme under One Factor Control

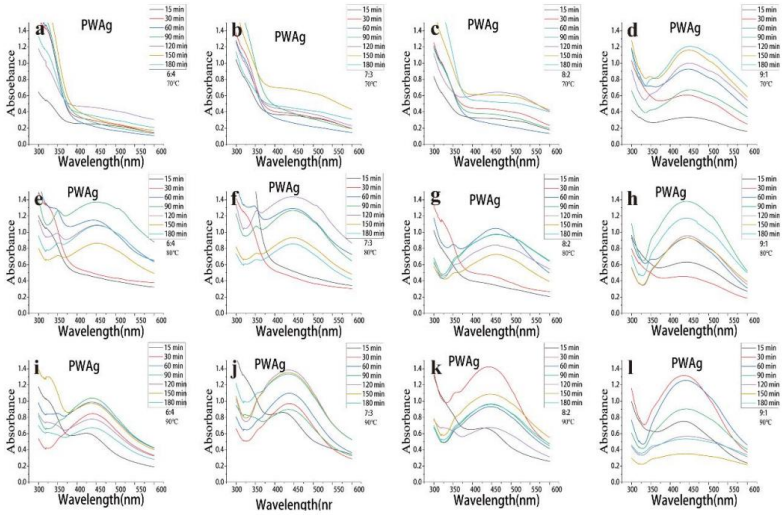

Figure 9. UV Spectra of Nanosilver Synthesized from Aqueous Extract of Patchouli under One Factor Control

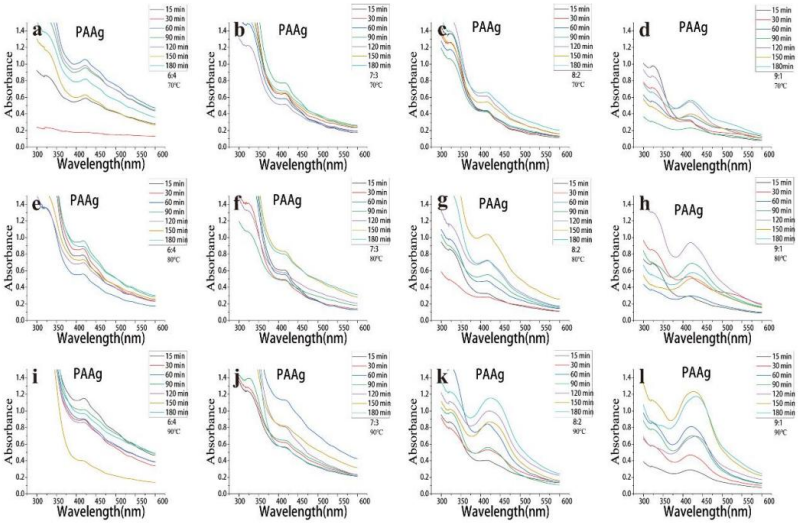

Figure 10. UV Spectra of Nanosilver Synthesized from the Alcoholic Extract of Patchouli under One-factor Control

3.3 Antibacterial Performance Results of Silver Nanoparticles

The microorganisms in the biofilm were isolated and purified, and the purified colonies were observed by Gram staining and microscopy. Under microscopic observation, the bacterial strains appeared red and purple-blue, respectively (Figure 11), indicating the successful isolation of Escherichia coli, Staphylococcus aureus, Aspergillus niger, and Aspergillus flavus.

Figure 11 shows the antibacterial effects of silver nanoparticles and benzalkonium chloride on the microbial strains. Regarding bacterial inhibition (Figures 12 and Table 1), CAAg exhibited the most significant inhibitory effect against E. coli and S. aureus, with inhibition zone diameters of 23.73 mm

and 23.30 mm, respectively. In contrast, TWAg showed the weakest inhibitory effect against E. coli, while the chemical biocide BC showed the weakest inhibitory effect against S. aureus, with an inhibition zone diameter of 17.73 mm. Most silver nanoparticles and benzalkonium chloride exhibited slightly stronger inhibitory effects against E. coli than against S. aureus; however, silver nanoparticles synthesized from both aqueous and alcoholic extracts of agastache showed the opposite trend, which may indicate that agastache-synthesized silver nanoparticles are more sensitive to S. aureus.

In terms of fungal inhibition, CWAg exhibited the best inhibitory effects against A. niger and A. flavus, with inhibition zone diameters of 22.67 mm and 27.93 mm, respectively. In contrast, BC showed poor inhibitory effects against both fungi, producing the smallest inhibition zones, indicating that the chemical biocide is less effective than plant-synthesized silver nanoparticles in antifungal activity. The biocides did not show a pattern similar to that observed for bacteria when treating fungi. Meanwhile, there was no clear advantage of aqueous extracts over alcoholic extracts or vice versa in inhibiting the four microorganisms.

Overall, the plant-synthesized silver nanoparticles exhibited strong inhibitory effects against all selected bacteria and fungi at low concentrations, outperforming the chemical biocide BC.

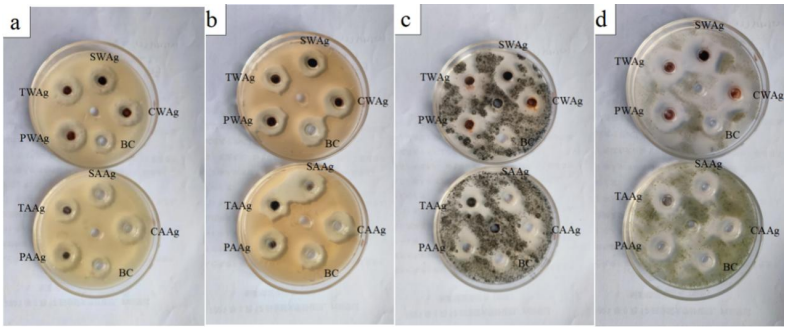

Figure 11. Actual Diagram of the Ring of Inhibition Produced by a Fungicide

Table 1 Results of Bacteriostatic Activity of Fungicides

	Zone of inhibition (mm)			
	E. coli	***S. aureus***	***A. niger***	*A. flavus*
CWAg	22.37±0.50	22.03±0.90	22.67±0.41	27.93±0.35
CAAg	23.73±0.72	23.30±0.87	22.10±0.75	20.57±0.61
SWAg	21.33±0.61	20.80±0.85	20.50±0.62	25.50±0.67
SAAg	23.20±0.56	20.10±0.75	21.23±0.55	20.33±0.47
TWAg	20.70±0.81	20.57±1.24	18.20±0.36	23.57±0.65
TAAg	22.13±0.34	20.07±0.91	20.03±0.47	20.90±0.26
PWAg	23.00±0.67	23.10±0.95	20.63±0.64	25.17±0.38

PAAg	21.57±0.55	22.23±0.66	19.93±0.33	21.27±0.62
BC	21.97±0.24	17.73±0.20	14.03±0.35	19.07±0.24

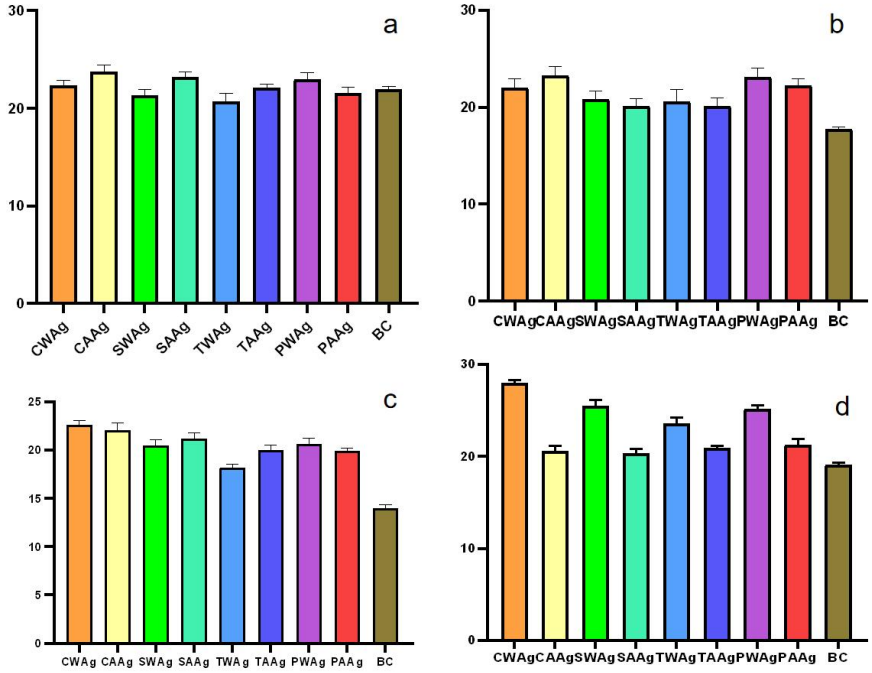

Figure 12. Significance Analysis of Bacteriostatic Activity

3.4 Evaluation of Antibacterial Activity of Silver Nanoparticles

Numerous studies have confirmed that silver nanoparticles prepared using plant extracts as reducing agents possess significant antifungal and antibacterial activities. As shown in Table 1 and Figure 12, although low concentrations of silver nanoparticles were used, their efficacy against Escherichia coli, Staphylococcus aureus, Aspergillus niger, and Aspergillus flavus was generally superior to that of benzalkonium chloride. Silver nanoparticles can destroy the cell membranes, genetic factors, and nutrient transport channels of microorganisms, leading to microbial death. The bactericidal mechanism of benzalkonium chloride mainly lies in its ability to alter the permeability of microbial cell membranes, causing leakage of cellular contents and thereby killing the microorganisms. Furthermore, because the peptidoglycan layer of Gram-positive bacteria enhances the rigidity of the cell wall and protects the microorganisms from osmotic lysis, they are generally more resistant to biocides than Gram-negative bacteria. Therefore, in this experiment, the inhibitory effects of plant-synthesized silver nanoparticles and benzalkonium chloride on E. coli were weaker than those on S. aureus.

By optimizing synthesis parameters, silver nanoparticles synthesized using thyme aqueous extract produced nanoparticles of 10–20 nm, resulting in inhibition zone diameters of 16 mm and 18 mm against E. coli and S. aureus, respectively. In another study on silver nanoparticles synthesized using

thyme, it was found that 90 nm silver nanoparticles exhibited low antibacterial activity against E. coli, with a minimum inhibitory concentration of 40 μg/mL against S. aureus. These findings are inconsistent with the results of the present experiment, indicating that the antibacterial activity of plant-synthesized silver nanoparticles may be influenced by multiple factors, including reaction temperature, concentration of plant extracts, and reaction time. In this experiment, except for the benzalkonium chloride group, the differences in inhibition zone diameters among different silver nanoparticles against the two bacterial species were relatively small. However, there were certain differences in the inhibitory effects of various silver nanoparticles against fungi. For example, SWAg showed poor antibacterial activity, which may be attributed to its larger particle size or the lack of synergistic effects from oxygen-containing components, thereby affecting the generation of reactive oxygen species and leading to poor bactericidal efficacy.

Furthermore, studies have indicated that the aqueous and alcoholic extracts of mint differ in composition, with the alcoholic extract containing tannins, sterols, and anthocyanins. It has been speculated that this may explain the higher antifungal activity of the alcoholic extract against Candida albicans. In the present experiment, although the antibacterial activities of silver nanoparticles synthesized from aqueous and alcoholic extracts of four plant species were compared, no regular pattern was observed in the results. This suggests that the antibacterial efficacy of silver nanoparticles synthesized from plant aqueous and alcoholic extracts may depend on the microbial species. Therefore, the conclusions of this experiment can serve as a reference, but when applied in practice, the results may vary depending on the types of microorganisms present.

4. Conclusion

Fungal and bacterial growth is one of the key factors contributing to the deterioration of stone buildings in Yunfeng Tunpu, among which Escherichia coli, Staphylococcus aureus, Aspergillus niger, and Aspergillus flavus are common local microbial communities. In this study, silver nanoparticles were synthesized using aqueous and alcoholic extracts of four plant species. The experimental results showed that these plant-synthesized silver nanoparticles exhibited significant antibacterial effects against common microorganisms on stone buildings, with those synthesized from cinnamon extract performing most prominently. The removal efficacy of the silver nanoparticles synthesized from these four plants was generally superior to that of benzalkonium chloride. This finding reveals the great potential of using plant-synthesized silver nanoparticles as an effective and non-toxic antibacterial agent in cultural heritage conservation.

References

DENG, S., & TING, Y. P. (2005). Characterization of PEI-modified biomass and biosorption of Cu(II), Pb(II) and Ni(II). *Water Res*, *39*(10), 2167-77.

FAN, Y., LI, Y., LI, H. et al. (2018). Evaluating heavy metal accumulation and potential risks in

soil-plant systems applied with magnesium slag-based fertilizer. *Chemosphere*, *197*, 382-8.

FU, Z. J., JIANG, S. K., CHAO, X. Y. et al. (2022). Removing miscellaneous heavy metals by all-in-one ion exchange-nanofiltration membrane. *Water Res*, *222*, 118888.

AN, X., WU, Z., SHI, W. et al. (2021). Biochar for simultaneously enhancing the slow-release performance of fertilizers and minimizing the pollution of pesticides. *Journal of Hazardous Materials*, *407*, 124865.

ANAE, J., AHMAD, N., KUMAR, V. et al. (2021). Recent advances in biochar engineering for soil contaminated with complex chemical mixtures: Remediation strategies and future perspectives. *Science of The Total Environment*, *767*, 144351.

BOUSKOUT, M., BOURHIA, M., AL FEDDY, M. N. et al. (2022). Mycorrhizal Fungi Inoculation Improves Capparis spinosa's Yield, Nutrient Uptake and Photosynthetic Efficiency under Water Deficit. *Agronomy*, *12*(1), 149.

HAN, F., AN, S-Y, LIU, L. et al. (2023). Simultaneous enhancement of soil properties along with water-holding and restriction of Pb–Cd mobility in a soil-plant system by the addition of a phosphorus-modified biochar to the soil. *Journal of Environmental Management*, *345*, 118827.

HOU, R., ZHU, B., WANG, L. et al. (2024). Mechanism of clay mineral modified biochar simultaneously immobilizes heavy metals and reduces soil carbon emissions. *Journal of Environmental Management*, *361*, 121252.

HUANG, Y., LI, T., WU, C. et al. (2015). An integrated approach to assess heavy metal source apportionment in peri-urban agricultural soils. *J Hazard Mater*, *299*, 540-9.

JOHNSON, A. W., GUTIERREZ, M., GOUZIE, D. et al. (2016). State of remediation and metal toxicity in the Tri-State Mining District, USA. *Chemosphere*, *144*, 1132-41.

KAJAL, S., & THAKUR, S. (2024). Coexistence of microplastics and heavy metals in soil: Occurrence, transport, key interactions and effect on plants. *Environ Res*, *262*(Pt 2), 119960.

KANDELER, E., TSCHERKO, D., BRUCE, K. D. et al. (2000). Structure and function of the soil microbial community in microhabitats of a heavy metal polluted soil. *Biology and Fertility of Soils*, *32*(5), 390-400.

KAYAMA, M., & YAMANAKA, T. (2024). Growth characteristics of ectomycorrhizal seedlings of Quercus glauca, Quercus salicina, and Castanopsis cuspidata planted on acidic soil. *Trees*, *28*(2), 569-583.

LENG, L. J., YUAN, X. Z., ZENG, G. M. et al. (2015). Surface characterization of rice husk bio-char produced by liquefaction and application for cationic dye (Malachite green) adsorption. *Fuel*, *155*, 77-85.

LI, B., LI, K., & LI, X. (2024). Fabrication of abundantly functionalized dendritic biochar composites as adsorbents for the high-efficiency removal of heavy metal ions and dyes. *Separation and Purification Technology*, *337*, 126368.

LI, H., QU, Y., WANG, Z. et al. (2022). Passivation Remediation of Cadmium Contaminated Soil by

Polyethyleneimine Modified Biochar. *Research Square*.

LI J, GAO Y, LI C, et al. Pristine and Fe-functionalized biochar for the simultaneous immobilization of arsenic and antimony in a contaminated mining soil [J]. Journal of Hazardous Materials, 2024, 469: 133937.

LIANG, M., LU, L., HE, H. et al. (2021). Applications of Biochar and Modified Biochar in Heavy Metal Contaminated Soil: A Descriptive Review. *Sustainability*, *13*(24), 14041.

LIU, H. W., DONG, Y. H., WANG, H. Y. et al. (2010). Ammonium adsorption from aqueous solutions by strawberry leaf powder: Equilibrium, kinetics and effects of coexisting ions. *Desalination*, *263*(1-3), 70-75.

LIU, Z., XU, Z., XU, L. et al. (2022). Modified biochar: Synthesis and mechanism for removal of environmental heavy metals. *Carbon Research*, *1*(1).

LONG, Z., WU, Y., ZHU, H. et al. (2024). Environmental protection measures mitigate Pb but not Cd accumulation in soils: Evidence from a 49-year soil chronosequence in an industrial and mining city in Southwest China. *J Hazard Mater*, *478*, 135441.

MA, X., ZHU, B., NIE, Y. et al. (2021). Root and mycorrhizal strategies for nutrient acquisition in forests under nitrogen deposition: A meta-analysis. *Soil Biology and Biochemistry*, *163*, 108418.

MAI, X., TANG, J., TANG, J. et al. (2025). Research progress on the environmental risk assessment and remediation technologies of heavy metal pollution in agricultural soil. *J Environ Sci (China)*, *149*, 1-20.

MARCIŃCZYK, M., KRASUCKA, P., DUAN, W. et al. (2024). Effect of zinc-biochar composite aging on its physicochemical and ecotoxicological properties. *Environ Pollut*, *341*, 122856.